Nonplanar, Supersonic, Three-Dimensional, Oscillatory, Piecewise Continuous-Kernel Function Method

I. Lottati* and E. Nissim†
Technion—Israel Institute of Technology, Haifa, Israel

The three-dimensional, supersonic, piecewise continuous-kernel function method formulated for studying oscillatory and steady flows is hereby extended to cope with nonplanar configurations in the supersonic region. This work treats problems associated with the computation of the kernel function for the nonplanar supersonic case and the anomalies associated with almost adjoining lifting surfaces. Interference aerodynamic forces as computed by the present method are compared with results obtained using other numerical methods. The reverse flow theorem is also used to indicate the accuracy of the computed results.

Introduction

SUPERSONIC numerical lifting surface methods can be divided into three categories: those that adopt 1) the velocity potential, 2) the gradient of the velocity potential, and 3) the acceleration potential. Typical of the first method is the Mach-box[1-3] method, whose shortcomings include the fact that the velocity potential must be determined off the planform in the so-called diaphragm regions and the treatment of the "jagged" leading and trailing edges cause difficulties in obtaining a converged solution. The velocity potential-collocation methods[4] eliminate the diaphragm region ahead of subsonic edges, but it appears that substantial computational labor is involved and that some computational problems remain which affect the level of accuracy of the results.

Jones and Appa[5] applied the gradient of the velocity potential to develop a code for computing aerodynamic forces on lifting surfaces in supersonic flow. The potential-gradient method (PGM) has shown promise of this approach to compute interfering nonplanar configurations. The method permits an exact idealization of the planforms, without any need for assumption of pressure distribution mode shapes. However, Ref. 5 is limited by a series expansion that ceases to be valid in the higher-frequency domain, as well as for the low supersonic Mach numbers (toward unity). Hounjet[6] improved the method by using Laschka's exponential series expansion scheme to represent the supersonic kernel. Although Hounjet has improved the validity of PGM, there is still a requirement for a large number of panel elements for convergence of the results. An improvement in the method was recently made by Chen and Liu,[7] extending the method for efficient use in the higher-frequency domain. This extension is reported to improve the accuracy of the results, and it reduces the panel number substantially compared to Refs. 5 and 6. An improved version of PGM was developed by Appa[8] in which, by rearrangement of certain terms, an integral relation between the downwash and the potential gradient has been derived, which obviates the need to consider wake elements. The results reported in Ref. 8 are preliminary and relate to isolated wings only. The PGM method was also applied by Giesing and Kalman[9] to develop a supersonic oscillatory doublet-lattice code.

Received Dec. 6, 1985; revision received Aug. 22, 1986.

*Senior Lecturer, Department of Aeronautical Engineering.
†Professor, Department of Aeronautical Engineering. Member AIAA.

The kernel function method[10,11] belongs to the third category. The use of the kernel function method (KFM) requires the user to represent the pressure distribution over the wing in terms of pressure functions. It requires, therefore, a full knowledge of all pressure discontinuities existing over the lifting surface and along their boundaries;[12] in other words, a good knowledge of the characteristics of the unknown solution must be known. In addition, the accuracy and convergence of the results depend on the location of the collocation points over the wing and on whether the integration techniques take full account of the various singularities of the pressure and of the kernel. For these reasons, the use of the KFM is often considered as cumbersome and lacking in generality. However, the results of those kernel function applications that permit taking full account of the above-mentioned points are characterized by a high level of accuracy and rapid convergence. The supersonic pressure distribution on a wing is known to have discontinuity either in pressure or in the gradient of the pressure along the Mach lines. These discontinuities are due to the propagation of information in the supersonic flow region, which is governed by a hyperbolic differential equation type. Cunningham's method[10,11] accounts for these discontinuities by assuming a series of continuous functions for the pressure distribution weighted by a supersonic weighting function. The supersonic weighting function (which is discontinuous) is based on conical flow theory solutions to the lift distribution on flat swept wings.[13] No secondary reflections of the Mach lines are accounted for, and obviously the weighting functions are limited to the few flow examples that can be solved analytically. Ueda and Dowell[14] developed the doublet-point method, which models the wing as a system with a finite number of points of the acceleration potential doublet. The method is very simple and easy to apply, though there are some inherent problems in it. For example, the pressure distribution has strong fluctuations on wings that have highly swept leading edges since the modeling of the wing is equivalent to a wing with a jagged configuration at its leading edge. To reduce the jagged configuration, one needs to use a finer lattice, which leads to a very large number of panels and unknowns.

The formulation of the piecewise continuous-kernel function method[15-17] (PCKFM) for subsonic and supersonic flows was intended to overcome most of the above-mentioned problems associated with the KFM. In the present work, the extension of the PCKFM to compute aerodynamic forces on a nonplanar configuration in supersonic flow is described. It is assumed that the reader is familiar with the PCKFM and with its previous applications. The present work treats, therefore,

only those problems associated with the computation of the kernel function for the nonplanar supersonic case and the anomalies associated with almost adjoining lifting surfaces. Numerical examples are presented. Due to the scarcity in the current literature of available examples relating to supersonic nonplanar configurations, accuracy of the results needs assessment. This is done by applying the reverse flow theorem as well.[18-20]

Brief Description of the Nonplanar PCKFM

In general, PCKFM[15-17] can successfully cope with unknown pressure singularities, provided their location is known. The wing surface is therefore divided into boxes in such a way that pressure singularities are permitted along the boundaries of the boxes. Unlike the doublet-lattice method,[21] the boxes used by the PCKFM can (and are preferred to) be as large as possible, provided they prevent pressure discontinuities (implying also discontinuities in the derivatives of the pressure) from lying within the regions defined by the boundaries of the boxes. The pressure distribution in each box is then represented by a set of continuous polynomials spanning the regions between adjoining singularities. In order to accelerate convergence, pressure singularities are assumed to be known only along the boundaries of the wing or, more specifically, the form of the leading edge (LE), trailing edge (TE), and wing-tip pressure singularities are assumed to be known and are treated in the analysis as such. All other pressure singularities are ignored during the analysis, and their consideration is limited to the determination of the boundaries among the different boxes. Discontinuities of pressure or gradient of the pressure distribution over the lifting surfaces are expected to occur along the Mach lines. Thus, the limits of the boxes are determined according to the Mach line configuration over the wing (see Fig. 1). This means that the geometry of the panels is a function of the Mach number of the flow. The fact that the wing is divided into panels according to the Mach lines increases the accuracy and credibility of the results though the data base for the code has to be changed for each Mach number to be computed. The problems associated with the basic three-dimensional PCKFM were treated thoroughly in Refs. 15–17. Only additional problems that arise from the three-dimensional nonplanar flow configurations and that require the formulation of numerical techniques for the successful application of the method in the nonplanar supersonic flow are addressed in this paper.

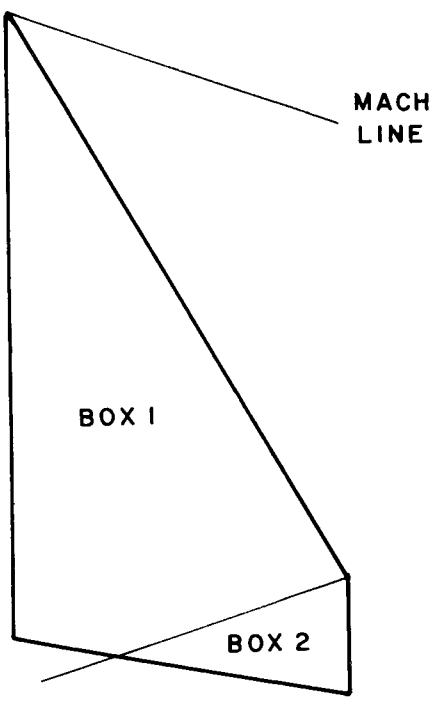

Fig. 1 Box allocation on a subsonic LE, clipped delta wing.

Figure 1 shows an example of a box allocation on a wing with subsonic LE and supersonic TE. The wing is divided into two boxes that are separated by the Mach lines. The pressure singularities considered in the analysis are the subsonic-LE-type singularity and the singularity of the gradient of pressure at the tip. All other singularities (including the singularity along the Mach line) fall within the category of ignored singularities, since they lie along the boundaries of the boxes and not along the boundaries of the wing. The pressure distribution in each of the boxes formed by the PCKFM can, therefore, be represented in general terms by the following expression:

$$\frac{\Delta p(\xi,\eta)}{q} = \sum_{j=1}^{ns} \sum_{i=1}^{nc} A_m W(\eta) P_j(\eta) w(\xi) p_i(\xi)/c(\eta) \quad (1)$$

where $\Delta p(\xi,\eta)$ represents the distribution of the pressure difference across the box, $q=\rho v^2/2$ the dynamic pressure, A_m is a scalar coefficient, nc and ns are the number of chordwise and spanwise pressure polynomials, respectively, and $m=(j-1)*nc+i$. The parameters ξ and η represent coordinates in the chordwise and spanwise directions, respectively. $W(\eta)$ and $w(\xi)$ represent the assumed wing boundary singularities in the chordwise and spanwise directions, respectively. Each polynomial $p_i(\xi)$ and $P_j(\eta)/c(\eta)$ is orthogonal to its respective weight function $w(\xi)$ and $W(\eta)$, where the pressure is normalized by the local chord $c(\eta)$.

The relationship between the pressure distribution over the wing and its resulting downwash is given by

$$\frac{\tilde{W}(x,y,z)}{v} = \frac{1}{8\pi} \int \int_S \frac{\Delta p(\xi,\eta)}{q} \frac{K_p(x-\xi,y-\eta,z-\zeta,k,M)}{r^2} d\xi d\eta \quad (2)$$

where

$\tilde{W}(x,y,z)/v$ = vertical nondimensional velocity [downwash at any collocation point (x,y,z) on the wing]
$K_p(\ldots)$ = modified kernel function (without the second-order pole) that relates the downwash at the collocation point (x,y,z) caused by a unit pressure difference at point (ξ,η,ζ)
$k=\omega b/v$ = reduced frequency (ω is the frequency of oscillation and b a reference length)
M = Mach number
S = area of the wing configuration
$r^2=(y-\eta)^2+(z-\zeta)^2$ = second-order pole for the coplanar and almost coplanar interference configuration
x,y,z = coordinates of the collocation point
ξ,η,ζ = coordinates of the doublet point

The kernel function for the supersonic case $K_p(\ldots)$ was given by Harder and Rodden[22] in a form similar to that given earlier by Landahl[23] for subsonic flow. In the derivation of the nonplanar supersonic kernel function based on the acceleration potential, Harder and Rodden[22] performed the differentiation to obtain the downwash at the control point prior to integration of the kernel function-pressure function product, as is normally done in deriving the acceleration potential kernel function. This resulted in a (3/2) power singularity along the Mach hyperbola (see Fig. 2) on any surface that was not coplanar with the control point. Such a singularity cannot be integrated, and the original derivation provided no means for

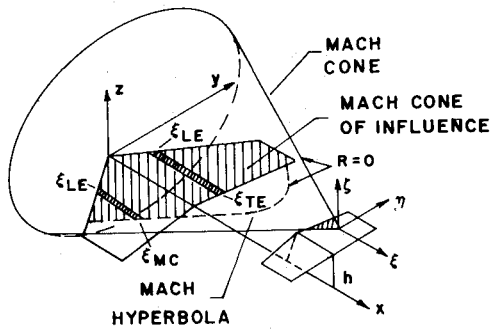

Fig. 2 Domain of influence for a nonplanar wing-tail configuration.

defining the finite part of the improper integral. This peculiarity of the supersonic nonplanar kernel function was observed by Cunningham[10] in the process of developing the subroutine for computing oscillatory supersonic aerodynamics on interfering surfaces. This key issue is considered in the following.

The potential at point (x,y,z) for a supersonic doublet due to a pressure difference Δp at (ξ,η,ζ) directed in the positive z direction is as follows (for the steady case):

$$\varphi(x_0,y_0,z_0) = -(v\Delta p/4\pi\rho)\,[z_0 x_0 D(x_0-\beta r)/r^2 R] \tag{3}$$

where

$$x_0 = x-\xi,\ y_0 = y-\eta,\ z_0 = z-\zeta,\ \beta = \sqrt{M^2-1},\ R^2 = x_0^2 - \beta^2 r^2$$

and

$$D(x_0-\beta r)\begin{cases} =1, & x_0 \geq \beta r \\ =0, & x_0 < \beta r \end{cases} \tag{4}$$

The total potential at (x,y,z) due to a Δp distribution on the wing is given by the integral over the surface S of the wing, as follows:

$$\phi(x,y,z) = -\frac{v}{4\pi\rho}\int\int_S \Delta p \frac{z_0 x_0 D(x_0-\beta r)}{r^2 R}\,\mathrm{d}\xi\,\mathrm{d}\eta \tag{5}$$

The downwash in the z direction at point (x,y,z) is then

$$\tilde{W}(x,y,z) = \frac{\partial}{\partial z}\phi(x,y,z) \tag{6}$$

In the kernel function formulation, following Harder and Rodden[22] and Landahl,[23] differentiation is performed before integration. The interchange is permissible as long as the limits of integration are not a function of the variable of differentiation, which in this case is z.

For coplanar surfaces in supersonic flow, the limits of integration (on the surface S) are defined by the geometry of the planform and the forward Mach cone whose location is independent of z. For nonplanar configurations, the Mach cone boundary is a hyperbola (see Fig. 2) whose location is a function of z for a fixed ζ. Thus, performing the differentiation of the integral in Eq. (6) has to be done while applying Leibnitz' rule, as was pointed out by Cunningham[10]:

$$\frac{\partial}{\partial z}\phi(x,y,z) = -\frac{v}{4\pi\rho}\frac{\partial}{\partial z}\int_{\eta_1}^{\eta_2}\int_{\mathrm{LE}}^{\mathrm{MC}} \Delta p\ \varphi(x_0,y_0,z_0)\,\mathrm{d}\xi\,\mathrm{d}\eta \tag{7}$$

where η_1,η_2 are the spanwise limits defined by the Mach cone intersection with the planform boundary (both functions of z). The limits ξ_{LE} and ξ_{MC} are the leading edge and Mach hyperbola boundaries (or trailing edge, see Fig. 2). The value of ξ_{MC}, if determined by the forward Mach hyperbola boundary, is a function of z. Thus, the fact that η_1 and η_2 and ξ_{MC} (if determined by Mach hyperbola) are a function of z should be taken into account while performing the differentiation of Eq. (7) according to Leibnitz' rule. In Ref. 10, Cunningham performed the differentiation of Eq. (7) analytically. To alleviate the complexity of the calculus, Cunningham[10] assumed that $\partial\eta_1/\partial z$ and $\partial\eta_2/\partial z$ are negligible, and he concentrated on dealing with the $\partial\xi_{\mathrm{MC}}/\partial z$ term. In spite of these simplifying assumptions, the expressions obtained in Ref. 10 are very complex and cumbersome. In order to avoid similar difficulties in the present work, it was decided to try and perform the differentiation in Eq. (7) numerically. If successful, this approach will obviously take into account all the extra nonzero terms required by Leibnitz' rule that have hitherto been neglected. Following Ref. 24, for the unsteady nonplanar case, Eq. (2) can be rewritten

$$\frac{\tilde{W}(x,y,z)}{v} = \frac{\partial}{\partial N}\int\int_S \frac{\Delta p(\xi,\eta,\zeta)}{8\pi q}\frac{\partial}{\partial n}\left[\exp(-i\omega x_0/v) \times \int_{-\infty}^{x_0}\frac{\exp(-i\omega(\lambda - MR')/v\beta^2)}{R'}\mathrm{d}\lambda\right]\mathrm{d}\xi\,\mathrm{d}\eta \tag{8}$$

where λ is an integration parameter and where

$$R' = \sqrt{\lambda^2 - \beta^2(y_0^2+z_0^2)}$$

and

$$\frac{\partial}{\partial n} = \cos\gamma(\eta)\frac{\partial}{\partial\zeta} - \sin\gamma(\eta)\frac{\partial}{\partial\eta}$$
$$\frac{\partial}{\partial N} = \cos\gamma(y)\frac{\partial}{\partial z} - \sin\gamma(y)\frac{\partial}{\partial y} \tag{9}$$

where $\gamma(\ )$ is the lateral angle between the wing and the x-y plane at the point indicated within the parentheses (i.e., localized dihedral angle).

The expressions in Eq. (9) can be transformed to the following:

$$\frac{\partial}{\partial n} = [z_0\cos\gamma(\eta) - y_0\sin\gamma(\eta)]\left(\frac{1}{r}\right)\frac{\partial}{\partial r} = \sin[\delta-\gamma(\eta)]\frac{\partial}{\partial r}$$
$$\frac{\partial}{\partial N} = [z_0\cos\gamma(y) - y_0\sin\gamma(y)]\left(\frac{1}{r}\right)\frac{\partial}{\partial r} = \sin[\delta-\gamma(y)]\frac{\partial}{\partial r} \tag{10}$$

where $\delta = \tan^{-1} z_0/y_0$. Thus, the downwash is related to the pressure doublet in the form

$$\frac{\tilde{W}(x,y,z)}{v} = \sin[\delta-\gamma(y)]\frac{\partial}{\partial r}\int\int_S \frac{\Delta p(\xi,\eta,\zeta)}{8\pi q} \times \sin[\delta-\gamma(\eta)]\exp(-i\omega x_0/v)K_1/r\,\mathrm{d}\xi\,\mathrm{d}\eta \tag{11}$$

where $K_1(=r\partial I_0/\partial r)$ is defined in Ref. 25 (for numerical algorithm to compute K_1, see Ref. 17).

The derivative $\partial/\partial r$ in Eq. (11) is performed numerically. It should be mentioned that for the coplanar case, Eq. (11) is identical to Eq. (2) using the kernel function defined in Ref. 25 ($\partial\eta_1/\partial z = \partial\eta_2/\partial z = \partial\xi_{\mathrm{MC}}/\partial z = 0$ for the coplanar case). This

fact is applied to assess the accuracy of the numerical differentiation of Eq. (11); the coplanar configuration was computed by Eq. (2) and compared to results obtained using Eq. (11). The numerical differentiation is performed by increasing r by Δr and the difference between the values obtained from $r+\Delta r$ and r is divided by Δr. Table 1 shows the computed aerodynamic forces as influenced by the value of Δr. It is seen that the value of $(\Delta r/s)=1\times10^{-5}$, where s is the semispan of the configuration (given in Fig. 4), gives identical results to those obtained by the analytical kernel function method for a coplanar configuration. Additional results obtained by the two different computational algorithms yielded identical numerical values up to the third digit (a fraction of 1%), which confirm the accuracy of the numerical differentiation. As already stated, the numerical differentiation bypasses the need to apply Leibnitz' rule and simplifies the expression for computing the nonplanar kernel function. Obviously, the peculiarity of the supersonic nonplanar kernel function reported by Cunningham[10] does not exist in this formulation.

To avoid the rapid variation of sin $[\delta-\gamma(\eta)]$ for the case of almost coplanar surfaces (i.e., $z_0/y_0\ll1$), the spanwise special integration technique described in Ref. 17 is applied to perform the integration of Eq. (11).

A point that needs to be discussed while dealing with a nonplanar configuration is the influence of the Mach lines emanating from the forward lifting surface on the pressure distribution on the rear surface. The question to be asked is whether the Mach lines emanating from the forward lifting surface cause a discontinuity in the pressure distribution (or in the gradient of the pressure) on the rear surface. This issue may affect considerably the number and shape of the panels of the rear surface. It will be shown that the Mach lines emanating from the forward lifting surface do not cause pressure discontinuities (or discontinuities in the gradient of pressure) on the rear lifting surface. Thus, each lifting surface is divided according to the Mach lines emanating from its own surface. This fact means that the boxes are always defined as polygons.

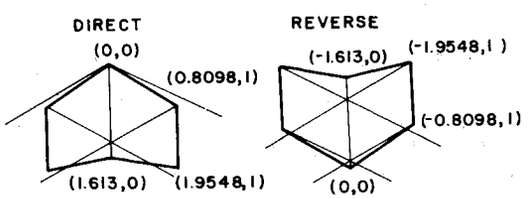

Fig. 3 Plan view of AGARD swept (isolated) wing.

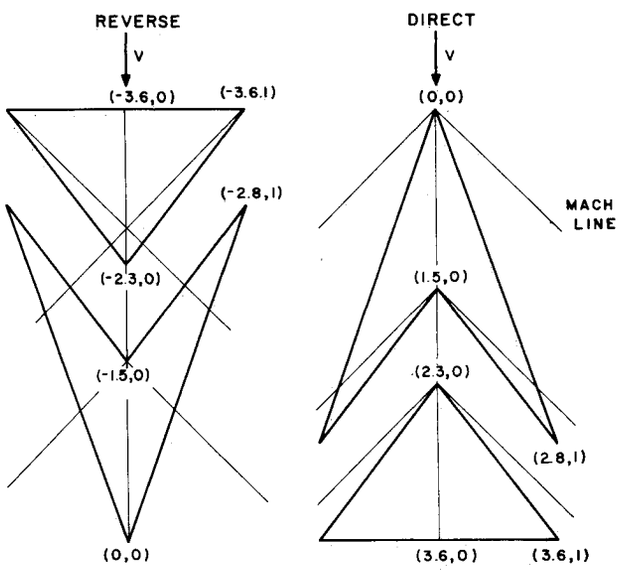

Fig. 4 Plan view of an interference wing-tail configuration.

Results

Even though numerous papers were written, backed by several computational methods on the evaluation of generalized air forces on configurations with interfering lifting surfaces, a need still exists for a reliable set of results to assess the accuracy of the computed numerical results in both planar and nonplanar configurations. It is sufficient to mention that the pressure distribution becomes extremely wavy and more difficult to predict accurately as the reduced frequency k gets larger and as the Mach number M approaches unity.

Convergence criteria are generally not available to enable the user to obtain the best results from a particular numerical method. Experimental methods are rarely available to verify the accuracy of predicted generalized forces developed on an oscillating interference configuration in supersonic flow. Thus, an attempt is made herein to use the reverse flow theorem[18-20] as a method to estimate the accuracy of the converged aerodynamic forces. It should be emphasized that the aerodynamic pressure distributions of lifting surfaces in the direct and reverse flows are totally different. Furthermore, the supersonic Mach cones of influence are changed drastically in the direct and reverse flow. It will therefore be assumed herein, despite our lack of formal proof regarding its correctness, that the numerical deviations between the integral values connecting forward and reverse flow pressure distributions is in itself indicative of the accuracy of the results obtained. Such an assumption was made in Ref. 19 regarding subsonic flows. In a recent study by van Niekerk,[26] some additional relations are produced between the forward and reverse flows on a lifting configuration. It also states that it is necessary that the pressure on the forward and reverse flow must be computed accurately to match numerically the existing relations between the forward and reverse generalized forces. To illustrate numerically our aforementioned assumption, the generalized forces are computed by PCKFM by allowing different sets of pressure polynomials in the direct and reverse flow and comparing the results to existing "exact" linearized results for those wings. Table 2 shows the results for two delta wings ($\mathcal{R}=1$ and $\mathcal{R}=6$) in steady flow, with $M=\sqrt{2}$. The results of Table 2 indicate that when the pressure on the wings is computed while assuming 1×1 (chordwise $\times$ spanwise) pressure polynomials per box, the lift is very different on the forward and reverse flows and obviously differs considerably from the "exact" linearized results. A better approximation of the aerodynamic pressure on wings is obtained by allowing a higher degree for the chordwise/spanwise pressure poly-

Table 1 Convergence study of the generalized forces as influenced by Δr while performing the numerical differentiation introduced in Eq. (11). The computed results are for the coplanar interference configuration given in Fig. 4.[a]

$\Delta r/s$	1×10^{-3}	1×10^{-4}	5×10^{-5}	1×10^{-5}	5×10^{-6}	1×10^{-6}	Coplanar kernel
$C_{L\alpha}$	1.154	1.942	1.953	1.956	1.956	1.956	1.956
$C_{M\alpha}$	−3.006	−4.174	−4.200	−4.208	−4.209	−4.209	−4.208

[a]The moment is about the configuration's apex; s is the semispan of configuration; the default value was taken as $\Delta r/s=1\times10^{-5}$.

Table 2 Convergence study of the lift in direct and reverse flow on two delta wings ($\mathcal{R}=1$ and $\mathcal{R}=6$), as influenced by the number of assumed pressure polynomials that represent the aerodynamic pressure for steady supersonic flow ($M=\sqrt{2}$)

Assumed pressure polynomials per box chordwise × spanwise	$C_{L\alpha}$ direct	$C_{L\alpha}$ reverse
Delta wing $\mathcal{R}=1$, "exact" linearized lift $C_{L\alpha}=1.465$		
1×1	1.522	1.975
2×2	1.478	1.585
3×3	1.475	1.481
Delta wing $\mathcal{R}=6$, "exact" linearized lift $C_{L\alpha}=4.000$		
1×1	3.594	5.209
2×2	4.143	4.057
3×3	4.034	4.052

Table 3 AGARD swept wing (Fig. 3) at $M=1.2$ in steady ($k=0$) and unsteady ($k=1$) flow in direct and reverse flow[a]

	$C_{L\alpha}$ steady	No. of boxes	No. of unknown	Percentage error
Direct	2.551	3	31	0.8
Reverse	2.530	5	34	
	C_{Lh} unsteady heave	No. of boxes	No. of unknown	Percentage error
Direct	2.608 (98.9°)	3	31	1.3
Reverse	2.640 (97.9°)	5	36	
	$C_{L\alpha}+ikC_{M\alpha}$ unsteady pitch	No. of boxes	No. of unknown	Percentage error
Direct	7.005 (9.5°)	3	31	0.5
Reverse	6.972 (9.8°)	5	36	

[a]The pitch axis is located at the configuration's apex.

nomials. Indeed, the results of Table 2 indicate that by assuming a higher order of pressure polynomials, the values obtained for the lift on the forward and reverse wings become closer and they approach the "exact" linearized results. Even though not proved mathematically, this numerical experiment indicates that if the computed generalized forces in the direct and reverse flows match within a reasonable numerical error, it is then reasonable to assume that the aerodynamic pressures are adequately represented. It should be noted that although the generalized forces computed by the PCKFM are of high accuracy (due to the fact that the pressure is represented by orthogonal polynomials in each box), the pressure distribution may still be inaccurate, due to its representation by a finite number of pressure polynomials. It will therefore be assumed in the following that the fulfillment of the reverse flow theorem relations might give an indication of the accuracy of the aerodynamic forces computed numerically.

It should be noted that the previous version of the PCKFM[16] was used to obtain results regarding isolated wings in supersonic flow for steady and oscillating wings. The results reported in Ref. 16 showed that the results obtained by the PCKFM compared very well with results obtained from the exact linearized theory for isolated wings. Unfortunately, there are no exact results for interfering surfaces, and the papers describing alternative codes for computing supersonic aerodynamic forces usually present results regarding isolated wings only. One of the few relevant examples in interfering

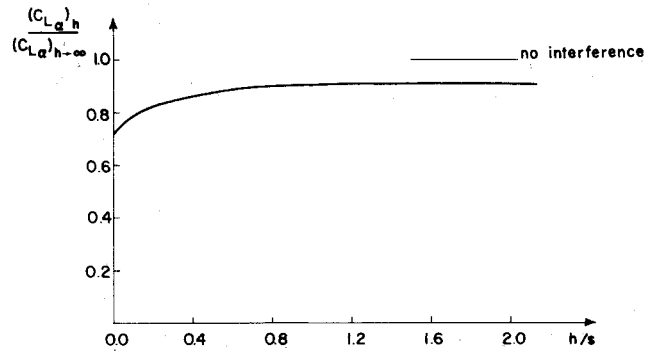

Fig. 5 Variation of the lift coefficient of nonplanar configuration (shown in Fig. 4) in steady flow vs the vertical difference between wing and tail computed by the PCKFM.

aerodynamics is given by Cunningham,[10,11] and it will be compared later in this paper.

The notation and formulation applied in this paper are the same as in Ref. 19. The aerodynamic forces obtained by direct and reverse flows are related in the following manner:

1) For steady flow, $C_{L\alpha}$, the lift coefficient for constant angle of attack, is identical for the direct and reverse flow.

2) For unsteady flow, the lift coefficient for wings oscillating in heave mode C_{Lh} is identical for the direct and reverse flow.

3) For unsteady flow, the lift and moment coefficients for wings oscillating in pitch, $C_{L\alpha}$ and $C_{M\alpha}$, respectively, in direct and reverse flow are related in the following form:

$$C_{L\alpha}+ikC_{M\alpha}=\bar{C}_{L\alpha}+ik\bar{C}_{M\alpha}$$

where $\bar{C}_{L\alpha}$ and $\bar{C}_{M\alpha}$ are the lift and moment coefficients obtained from the computed reverse flow.

For the sake of comparison of results with other existing computational methods and before embarking on configurations involving noncoplanar surfaces, the AGARD (isolated) swept wing (plotted in Fig. 3) is chosen to test the validity of the methods eventually to be employed herein. The results obtained when applying the PCKFM for direct and reverse flows are summarized in Table 3. The results displayed in Table 3 are organized in three parts: in the upper part, the results for the steady flow are shown. In the middle part, the results for the unsteady heave mode are shown and, in the last part, the results for the unsteady pitch mode are shown. The results obtained for the direct and reverse flow are in very good agreement in steady and unsteady cases. Without loss of generality, the reference length b (for the definition of the reduced frequency) is set to unity for convenience in all the numerical cases treated herein. It should be noted that the AGARD swept wing has a subsonic LE and supersonic TE for the direct flow, while in reverse flow the wing has supersonic LE and subsonic TE. Even though the pressure distribution on the wing differs appreciably for direct and reverse flows, the resulting total lift and moment fulfill the relations existing between the direct and reverse flows within acceptable numerical error (1-2%). For correlations with other methods, the generalized aerodynamic forces (with the definition of Ref. 7) for the AGARD swept wing as computed by different methods are displayed in Table 4. The results shown in Table 4 for the AGARD swept wing are typical for a comparison study conducted on a chosen configuration obtained by different computational methods and computed by different computers. It is very difficult to assess the efficiency and the accuracy of the results computed by the different codes. However, it is shown that the results obtained by the present method are in fairly good agreement with the results obtained by the various codes.

The idea of obtaining an indication regarding the computational errors using the differences between the forward and

Table 4 AGARD swept wing (Fig. 3), comparison of results obtained by different methods [$M=1.2$, $k=1$, and the three mode shapes are $H_1=1$, $H_2=x-c/2$, $H_3=(x-c/2)^2$][a]

	Method no of elements	Present (31)[b]	Present (21)	Ref. 7 (150)	Ref. 7 (100)	Ref. 6 (150)	Ref. 5 (147)	Ref. 29 (600)	Ref. 30 (1734)
Q_{11}	MOD	3.597	3.618	3.705	3.689	3.697	3.486	3.570	3.665
	ARG°	98.9	97.9	95.7	95.5	98.3	100.2	96.5	95.8
Q_{21}	MOD	0.889	0.874	0.930	0.934	0.891	1.012	0.868	0.904
	ARG°	145.8	144.3	143.1	142.1	143.4	147.8	144.7	143.0
Q_{31}	MOD	0.903	0.898	0.910	0.909	0.916	0.946	0.877	0.912
	ARG°	113.7	113.2	111.1	110.5	114.3	114.0	112.8	112.6
Q_{12}	MOD	4.417	4.401	4.502	4.479	4.575	4.492	4.370	4.490
	ARG°	24.0	23.0	21.4	21.4	24.0	25.0	21.2	21.0
Q_{22}	MOD	1.934	1.904	2.008	2.001	1.966	2.040	1.914	1.983
	ARG°	66.8	66.8	64.6	64.1	65.8	64.1	65.8	64.4
Q_{23}	MOD	1.287	1.262	1.298	1.306	1.335	1.291	1.255	1.313
	ARG°	44.3	44.5	43.6	44.0	45.4	41.5	43.5	43.5
Q_{13}	MOD	2.659	2.690	2.780	2.824	2.892	2.644	2.572	2.720
	ARG°	5.9	5.8	5.7	6.2	4.8	−0.3	3.5	3.7
Q_{23}	MOD	2.229	2.251	2.298	2.291	2.333	2.008	2.213	2.301
	ARG°	5.4	5.5	3.8	4.2	5.4	2.4	2.6	2.9
Q_{33}	MOD	1.283	1.304	1.378	1.393	1.378	1.218	1.270	1.346
	ARG°	21.9	22.2	21.1	20.7	20.0	24.9	20.1	19.9

[a] All the results except those relating to the present method were taken from Ref. 7. The generalized forces are normalized by area equal 2. To get the results of Table 3, the above have to be normalized by half the wing area ($S=2.758$). [b] Numbers in parentheses indicate number of elements.

Table 5 Interference configuration (Fig. 4) at $M=\sqrt{2}$ and $k=0$ in direct and reverse flow[a]

Vertical difference between surfaces	$C_{L\alpha}$ direct flow	$C_{L\alpha}$ reverse flow	Percentage error
Coplanar ($h=0$)	1.956	1.989	1.7
$h=0.1$	2.215	2.208	0.3
$h=0.2$	2.255	2.256	0.0
$h=0.4$	2.373	2.412	1.6
$h=0.6$	2.451	2.496	1.8

[a] 22 unknown for direct flow and 28 unknown in the reverse case.

reverse flows was further tested by applying the PCKFM to compute aerodynamic lift and moment coefficient for a delta wing ($\mathcal{R}=2$) with variable supersonic Mach numbers in steady flow, and the results obtained (not presented herein) for the direct and reverse flows were found to lie, in all cases, within the 2% error compared with the exact linearized results that exist for the steady flow case (the comparison between the present method and the exact linearized results was reported in Ref. 16).

Unfortunately, worked examples computed by other methods for nonplanar configurations in supersonic flow are very scarce. Thus, as mentioned, the reverse flow theorem will be applied to assess the accuracy of the computed results by the PCKFM. The first interference configuration to be tested is an arrow wing with a delta tail shown in Fig. 4 (in direct and reverse flow). The configuration has an $\mathcal{R}=1.43$ (referred to the total configuration area) and is tested at $M=\sqrt{2}$ in steady ($k=0$) and unsteady ($k=1$) flow for various vertical distances between the two surfaces. The results obtained for direct and reverse flow in the steady case are summarized in Table 5. Tables 6 and 7 display a comparison of the aerodynamic unsteady forces in direct and reverse flows for the same configuration shown in Fig. 4 when oscillating in heave and pitch modes. It is shown that the results computed for the direct and reverse flows, as indicated in Tables 5-7, compare very well, both for the steady and unsteady flow. The difference (error) between the computed direct and reverse flow aerodynamic coefficients is bounded within 2.5%, and this figure may indicate the accuracy of the present numerical method. It is worthwhile noting that there is a very steep increase in the lift coefficient between the coplanar ($h=0$) and almost coplanar ($h=0.1$) case in the steady flow, while in the unsteady flow the changes in the aerodynamic forces are very moderate. These same trends were reported in Refs. 17 and 27 for interfering configurations in subsonic flow. The efficiency of the method is pointed out by the low number of unknowns assumed for the pressure distribution on the configuration. The maximum computational labor is needed for computing an almost coplanar configuration due to the fact that the integration of Eq. (11) has to be done more accurately by using more integration points than otherwise (see Ref. 17). To represent some of the convergence characteristics of the aerodynamic coefficients as computed by the PCKFM, a convergence study of the lift coefficient of the nonplanar configuration shown in Fig. 4 ($h/s=0.1$) for various unknown pressure polynomials assumed for the tail is summarized in Table 8. It is seen that three polynomials in the chordwise and spanwise direction are usually the default value taken per box

Table 6 Interference configuration (Fig. 4) at $M=\sqrt{2}$ and $k=1$ in direct and reverse flow (heave mode)[a]

Vertical difference between surfaces	C_{Lh} direct flow, MOD (ARG°)	C_{Lh} reverse flow, MOD (ARG°)	Percentage error (modulus)
Coplanar ($h=0$)	2.759 (101.5)	2.704 (95.6)	2.0
$h=0.1$	2.643 (98.0)	2.592 (93.0)	2.0
$h=0.2$	2.572 (96.3)	2.528 (91.9)	1.7
$h=0.4$	2.474 (93.5)	2.420 (95.4)	2.2
$h=0.6$	2.401 (91.8)	2.380 (92.3)	0.9

[a]22 unknown for direct flow and 32 unknown in the reverse case.

Table 7 Interference configuration (Fig. 4) at $M=\sqrt{2}$ and $k=1$ in direct and reverse flow (pitch mode)[a]

Vertical differences between surfaces	$C_{L\alpha}+ikC_{M\alpha}$ direct flow, MOD (ARG°)	$C_{L\alpha}+ikC_{M\alpha}$ reverse flow, MOD (ARG°)	Percentage error (modulus)
Coplanar ($h=0$)	21.110 (4.1)	21.594 (1.1)	2.3
$h=0.1$	21.189 (1.3)	20.922 (−2.8)	1.3
$h=0.2$	20.672 (0.2)	20.497 (−3.4)	0.9
$h=0.4$	19.943 (−1.5)	19.751 (−4.7)	1.0
$h=0.6$	19.392 (−2.4)	19.438 (−5.6)	0.2

[a]22 unknown for direct flow and 32 unknown in the reverse case; pitch axis is located at the configurations apex.

Table 8 Convergence study of lift and moment coefficient of the nonplanar configuration shown in Fig. 4 (tail elevated $h=0.1$) for various unknown pressure polynomials assumed on the tail ($M=\sqrt{2}$, $k=0$)[a]

No. of pressure polynomials (PCKFM)		$C_{L\alpha}$	$C_{M\alpha}$
Chordwise	Spanwise		
2	2	1.907	−4.078
2	3	1.966	−4.242
3	3	2.215	−5.046
3	4	2.201	−5.017
4	4	2.203	−5.024

[a]The moment is about the configuration's apex; 13 unknown pressure polynomials assumed on the wing; the default for the assumed pressure polynomials is taken as 3 polynomials in the chordwise and spanwise direction per box.

Table 9 Interference configuration (Fig. 5) at $M=\sqrt{2}$ and $k=0$ in direct and reverse flow[a]

Vertical difference between surfaces	$C_{L\alpha}$ direct flow	$C_{L\alpha}$ reverse flow	Percentage error
Coplanar ($h=0$)	1.318	1.301	1.3
$h=0.1$	1.504	1.483	1.4
$h=0.2$	1.616	1.637	1.3
$h=0.4$	1.824	1.817	0.4
$h=0.6$	1.951	1.934	0.9

[a]38 unknown for direct flow and 40 unknown in the reverse case.

(the tail is taken as one box). Figure 5 depicts the variation of the steady lift coefficient (C_{L_α}) of the interference configuration (shown in Fig. 4) vs the vertical distance between the wing and tail in steady flow, as computed by the present method.

A more severe interference pattern configuration between two surfaces is shown in Fig. 6. The configuration has an $\mathcal{R}=0.741$ (referred to the total configuration area) and is tested at $M=\sqrt{2}$ in steady ($k=0$) and unsteady ($k=1$) flow. Tables 9–11 summarize the results obtained for the aerodynamic forces in both direct and reverse flows. These results

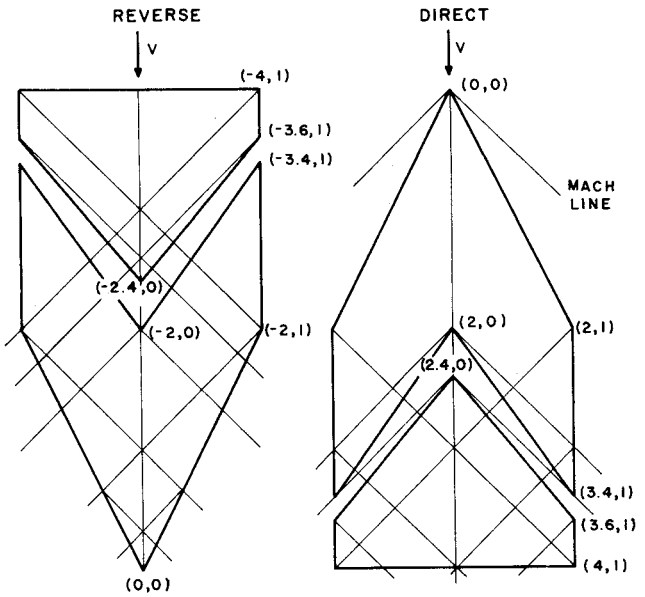

Fig. 6 Plan view of an interference wing-tail configuration.

are presented in the same format as those in Tables 5–7. Once again it is shown that the results computed for the direct and reverse flow, as indicated in Tables 9–11, compare very well (the error is found to lie within the 3% error), both for the steady and unsteady flow, even though the interference effects between the two surfaces are more pronounced than those occurring in the first configuration (Fig. 4). It should be noted that the pressure distribution and the gradient of the pressure on the rear surface are found to be continuous across the Mach lines that emanate from the forward lifting surface. This means that each surface can be divided into panels according to the Mach lines emanating from its own lifting surface. Thus, the shape of the panels is always polygonal. This assumption was tested on both configurations shown in Figs. 4

Table 10 Interference configuration (Fig. 5) at $M=\sqrt{2}$ and $k=1$ in direct and reverse flow (heave mode)[a]

Vertical difference between surfaces	C_{Lh} direct flow, MOD (ARG°)	C_{Lh} reverse flow, MOD (ARG°)	Percentage error (modulus)
Coplanar ($h=0$)	2.484 (111.7)	2.541 (111.3)	2.3
$h=0.1$	2.451 (107.5)	2.501 (108.0)	2.0
$h=0.2$	2.363 (105.6)	2.404 (105.6)	1.7
$h=0.4$	2.216 (102.4)	2.239 (103.2)	1.0
$h=0.6$	2.098 (100.7)	2.146 (103.9)	2.3

[a]38 unknown for direct flow and 47 unknown in the reverse case.

Table 11 Interference configuration (Fig. 5) at $M=\sqrt{2}$ and $k=1$ in direct and reverse flow (pitch mode)[a]

Vertical difference between surfaces	$C_{L\alpha}+ikC_{M\alpha}$ direct flow, MOD (ARG°)	$C_{L\alpha}+ikC_{M\alpha}$ reverse flow, MOD (ARG°)	Percentage error (modulus)
Coplanar ($h=0$)	20.598 (16.0)	20.826 (16.7)	1.1
$h=0.1$	20.210 (11.6)	20.421 (11.0)	1.0
$h=0.2$	19.680 (9.7)	19.519 (8.8)	0.8
$h=0.4$	18.499 (7.2)	18.502 (6.9)	0.0
$h=0.6$	17.508 (6.3)	17.253 (7.9)	1.5

[a]38 unknown for direct flow and 47 unknown in the reverse case; the pitch axis is located at the configuration's apex.

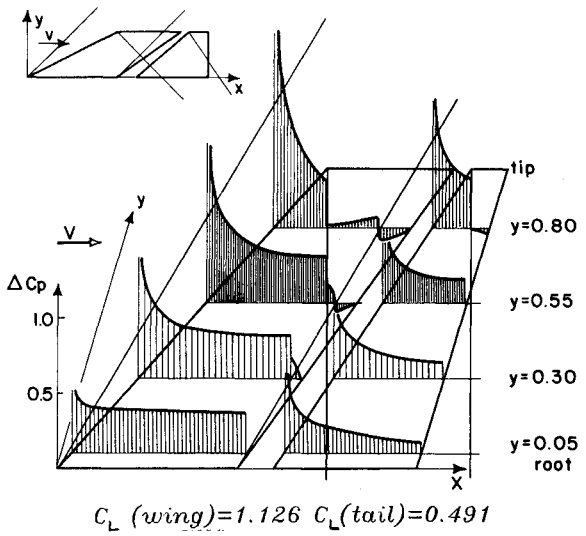

Fig. 7 Pressure distribution on an interfering nonplanar configuration in steady supersonic flow (tail elevation $h=0.2$, $M=\sqrt{2}$).

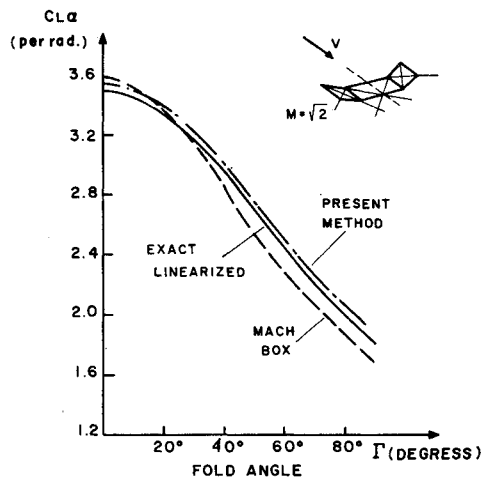

Fig. 8 Comparison of lift curve slope for an aspect ratio 4.0 rectangular wing with 50% folded tips in steady supersonic flow ($M=\sqrt{2}$), as computed by the present and MBOX methods and the exact linearized results.

and 6. Figure 7 shows a pressure distribution on the nonplanar configuration shown in Fig. 6 in steady flow ($M=\sqrt{2}$, $h=0.2$).

To demonstrate the ability of the present code to cope with lifting surfaces that have dihedrals, generalized aerodynamic lift coefficients are computed for an $AR=4$ rectangular wing with tips folded at 50% semispan at various fold angles Γ. For this configuration (tested at $M=\sqrt{2}$), Rodemich[28] developed an "exact" theoretical linearized steady-state solution. This configuration is one of the very few nonplanar interference examples for which an accurate result exists. Reference 2 compares the exact linearized solution of Rodemich[28] with results obtained while applying the Mach-box (MBOX) method. The $C_{L\alpha}$ values obtained by the PCKFM program at $M=\sqrt{2}$ are plotted vs fold angle Γ in Fig. 8, together with the exact linearized values obtained from Ref. 28 and the MBOX results from Ref. 2. It may be seen that the PCKFM values for the zero fold angle (planar rectangular wing) are very accurate as compared to the "exact" linearized value (0.8%) while the MBOX method yields results with good accuracy (2.5%). The results depicted in Fig. 8 indicate that the difference between the curve computed by PCKFM and the "exact" linearized diminished as the fold angle increases, pointing out the high accuracy of the results. The MBOX curve shows a higher value than the "exact" results for low fold angles ($\Gamma<20$ deg) and continues below the "exact" curve for higher fold angles ($\Gamma>20$ deg) while the difference between the curves increases as the fold angle increases (at $\Gamma=85$ deg the error is 6.75%). As stated, this example may serve as an example for testing the accuracy of the numerical code for nonplanar configurations, especially for the high fold angle, since "exact" linearized results do exist for this case. It is shown that the results obtained by the PCKFM are more accurate than the results ob-

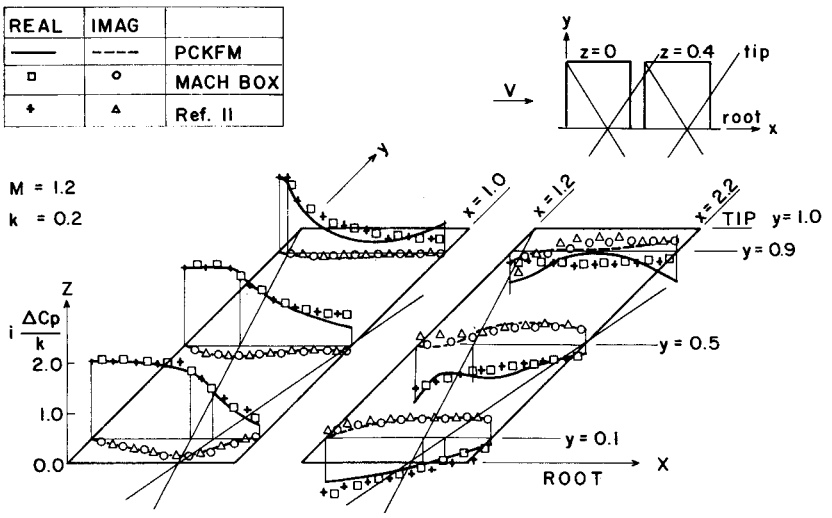

Fig. 9 Comparison of computed pressure distribution (by the present, MBOX, and Cunningham's methods) on a nonplanar rectangular (unswept) wing-tail configuration is unsteady supersonic flow.

tained for the MBOX method. This fact should be emphasized due to the fact that rectangular wings are well treated by the Mach-box approach.

Finally, Fig. 9 shows an illustration of the pressure distribution as obtained by the present method, together with a comparison of similar pressure distributions as obtained by the AFFDL Mach-box method and Cunningham's supersonic code. The configuration is a nonplanar wing-tail in supersonic flow at $k=0.2$ with a unit wing translation mode while the tail is stationary. Both the wing and the tail are rectangular surfaces ($AR=2$ based on the area of each lifting surface) with a semispan and chord of unity. The tail leading edge is 0.2 aft and 0.4 elevated above the wing trailing edge. To apply the PCKFM, the configuration is divided into 6 boxes (wing and tail, 3 boxes each according to the Mach lines shown in Fig. 9), and a total of 16 orthogonal polynomials are assumed to represent the pressure distribution on each lifting surface. The Mach-box solution is obtained by applying a total of 80 boxes on the configuration plus 109 boxes in the diaphragms. Cunningham[10,11] selects this problem for verifying his unsteady supersonic collocation nonplanar method, and it was on this example that the aforementioned peculiarity of the nonplanar supersonic kernel function was observed. The comparison of the pressure distributions displayed in Fig. 9 shows a similar tendency of the curves (computed by PCKFM, MBOX, and Cunningham[11]), even though there are slight discrepancies between them. It should be noted that at $M=1.2$ and $k=0.2$, it is expected that the pressure distribution will show some tendency toward waviness.[7] The PCKFM curves show a slightly wavy pressure distribution, especially on the rear lifting surface (shown in Fig. 9), as compared to the curves obtained by the Mach-box method and by Cunningham's method.

Conclusions

The PCKFM is tested, in this work, for nonplanar configuration both in steady and unsteady supersonic flows. The reverse flow theorem is used to yield an indication regarding the convergence and accuracy of the results. Unfortunately, worked examples computed by other methods for nonplanar configurations in supersonic flow are very scarce. Since it is very difficult to evaluate the accuracy of the approximate results obtained by different methods, especially when there are discrepancies between them, it is shown that the reverse flow theorem may be used to indicate (compatibly with the limitation of the reverse flow theorem) the accuracy of the results.

The extension of the PCKFM to the supersonic nonplanar configuration appears to yield results that are compatible with previous applications of the method. It yields converged results with a small number of unknown pressure polynomial coefficients and a minimum number of boxes, ensuring reduced computational labor, together with its inherent efficiency.

References

[1]Pines, S., Dugundji, J., and Neuringer, J., "Aerodynamic Flutter Derivatives for a Flexible Wing with Supersonic and Subsonic Edges," *Journal of the Aeronautical Sciences,* Vol. 22, Oct. 1955, pp. 693-700.

[2]Donato, V.W. and Huhn, C.R., "Supersonic Unsteady Aerodynamics for Wings with Trailing Edge Control Surfaces and Folded Tips," AFFDL-TR-68-30, Aug. 1968.

[3]Chipman, R.R., "An Improved Mach-Box Approach for the Calculation of Supersonic Oscillatory Pressure Distributions," *Proceedings of the AIAA/ASME/SAE 17th Structures, Structural Dynamics and Materials Conference,* May 1976, pp. 615-625.

[4]Appa, K., "Integrated Potential Formulation of Unsteady Supersonic Aerodynamics for Interacting Wings," AIAA Paper 75-762, May 1975.

[5]Jones, W.P. and Appa, K., "Unsteady Supersonic Aerodynamic Theory for Interfering Surfaces by the Method of Potential Gradient," NASA CR-2898, 1977.

[6]Hounjet, M.H.L., "An Improved Potential Gradient Method to Calculate Airloads on Oscillating Supersonic Interfering Surfaces," *Journal of Aircraft,* Vol. 19, May 1982, pp. 390-399.

[7]Chen, P.-C. and Liu, D.D., "A Harmonic Gradient Method for Unsteady Supersonic Flow Calculations," *Journal of Aircraft,* Vol. 22, May 1985, pp. 371-379.

[8]Appa, K., "A New Approach to Apply the Potential Gradient Method for Supersonic Unsteady Airload," AIAA Paper 85-0596, 1985.

[9]Giesing, J.P. and Kalman, T.P., "Oscillatory Supersonic Lifting Surface Theory Using a Finite Element Doublet Representation," AIAA Paper 75-761, 1975.

[10]Cunningham, A.M., "The Application of General Aerodynamic Lifting Surface Elements to Problems in Unsteady Transonic Flow," NASA CR-112264, Feb. 1973.

[11]Cunningham, A.M., "Oscillatory Supersonic Kernel Function Method for Interfering Surfaces," *Journal of Aircraft,* Vol. 11, Nov. 1974, pp. 664-670.

[12]Rowe, W.S., Winther, B.A., and Redman, M.C., "Prediction of Unsteady Aerodynamic Loading Caused by Leading Edge and Trailing Edge Control Surface Motion in Subsonic Compressible Flow-Analysis and Results," NASA CR-2543, Aug. 1975.

[13]Cohen, D., "Formulas for the Supersonic Loading, Lift and Drag of Flat, Swept-Back Wings with Leading Edges Behind the Mach Lines," NACA Rept. 1050, 1951.

[14]Ueda, T. and Dowell, E.H., "Doublet-Point Method for Supersonic Unsteady Lifting Surfaces," *AIAA Journal,* Vol. 22, Feb. 1984, pp. 179-186.

[15]Lottati, I. and Nissim, E., "Three-Dimensional Oscillatory Piecewise Continuous Kernel Function Method" (in three parts), *Journal of Aircraft,* Vol. 18, May 1981, pp. 346-363.

[16]Nissim, E. and Lottati, I., "Supersonic Three-Dimensional Oscillatory Piecewise Continuous Kernel Function Method," *Journal of Aircraft,* Vol. 20, Aug. 1983, pp. 674-681.

[17]Lottati, I. and Nissim, E., "Nonplanar, Subsonic, Three-Dimensional Oscillatory Piecewise Continuous-Kernel Function Method," *Journal of Aircraft,* Vol. 22, Dec. 1985, pp. 1043-1048.

[18]Flax, A.H., "Relations Between the Characteristics of a Wing and Its Reverse in Supersonic Flow," *Journal of the Aeronautical Sciences,* Vol. 16, No. 8, 1949, pp. 496-504.

[19]Lottati, I., "Reverse Flow Theorem Applied to Subsonic Unsteady Aerodynamic Forces," *Journal of Aircraft,* Vol. 23, Jan. 1986, pp. 95-96.

[20]Heaslet, M.A. and Spreiter, J.R., "Reciprocity Relations in Aerodynamics," NACA TN 2700, 1952.

[21]Albano, E. and Rodden, W.P., "A Doublet-Lattice Method for Calculating Lift Distributions on Oscillating Surfaces in Subsonic Flows," *AIAA Journal,* Vol. 7, Feb. 1969, pp. 279-285.

[22]Harder, R.L. and Rodden, W.P., "Kernel Function for Nonplanar Oscillating Surfaces in Supersonic Flow," *Journal of Aircraft,* Vol. 8, Aug. 1971, pp. 677-679.

[23]Landahl, M.T., "Kernel Function for Nonplanar Oscillating Surfaces in a Subsonic Flow," *AIAA Journal,* Vol. 5, May 1967, pp. 1045-1046.

[24]Vivian, H.T. and Andrew, L.V., "Unsteady Aerodynamics for Advanced Configuration. Part I. Application of the Subsonic Kernel Function to Nonplanar Lifting Surfaces," U.S. Air Force Flight Dynamics Laboratory, FDL-TDR-64-152, 1965.

[25]Rodden, W.P., "A Comparison of Methods Used in Interfering Lifting Surface Theory," AGARD Rept. No. 643, Supplement to the Manual on Aeroelasticity Vol. VI.

[26]Van Niekerk, B., "Computation of Second-Order Accurate Unsteady Aerodynamic Generalized Forces," *AIAA Journal,* Vol. 24, March 1986, pp. 492-498.

[27]Rodden, W.P., Gieseing, J.P., and Kalman, T.P., "New Developments and Applications of the Subsonic Doublet-Lattice Method for Nonplanar Configurations," AGARD Symposium on Unsteady Aerodynamics for Aeroelastic Analyses on Interfering Surfaces, Tonsberg, Norway, AGARD-CP-80-71, April 1971, pp. 4.1-4.27.

[28]Rodemich, E.R., "Analytical Solution of an Interference Problem in Supersonic Flow," North American Aviation, Inc. Rept. No. SID 65-695, June 1965.

[29]Stark, V.J.E., "Calculation of Aerodynamic Forces on Two Oscillatory Finite Wings at Low Supersonic Mach Numbers," SAAB TN.53, 1964.

[30]Fenain, M. and Guiraud-Vallée, D., "Numerical Calculations of Wings in Steady or Unsteady Supersonic Flow, Part 1: Steady Flows; Part 2: Unsteady Flow," *Recherche Aérospatiale,* No. 115, 1966-1967.